Dalton Transactions

ROYAL SOCIETY OF CHEMISTRY

PAPER

View Article Online
View Journal | View Issue

Cite this: *Dalton Trans.*, 2025, **54**, 14013

Structural diversities and magnetic properties of azido- and dicyanamido-bridged coordination polymers with 4,5-diphenylimidazole as a terminal ligand

Evangelia-Spyridoula Fotopoulou,[a] Nikos Panagiotou,[b] Anastasios J. Tasiopoulos,[b] Mark M. Turnbull,*[c] Spyros P. Perlepes*[a] and Vassilios Nastopoulos*[a]

With the aim of assessing the role and impact of pseudohalides on the molecular and supramolecular structures of copper(II)/heavily substituted imidazole complexes, the synthesis and characterization of the complexes $\{[Cu(N_3)_2(HL)]\}_n$ (**1**), $\{[Cu\{N(CN)_2\}_2(HL)]\cdot Me_2CO\}_n$ (**2**·Me_2CO) and $[Cu(NCO)_2(HL)_2]\cdot MeCN$ (**3**·MeCN) have been carried out; HL is the 4,5-diphenylimidazole ligand. The organic molecule behaves as a monodentate ligand through the pyridine-type nitrogen atom of the imidazole ring. The 1D polymer **1** is made up of undulating $\{-Cu-(N_3)_2-Cu-(N_3)_2-\}$ chains, with the HL ligands extending from both sides of the chains. The square pyramidal metal ions are alternately doubly bridged by two different types (basal–basal and basal–apical) of end-on azido groups. In **2**·Me_2CO, the $N(CN)_2^-$ ions behave as end-to-end (μ-1,5 or 2.101) ligands forming a 2D polymeric lattice, consisting of four-membered Cu^{II} rings interconnected by four dicyanamido bridges; the five-coordinate Cu^{II} ion adopts a geometry intermediate between square pyramidal and trigonal bipyramidal. The metal centre in the mononuclear complex **3**·MeCN is bonded to two HL ligands and two terminal isocyanato groups; the coordination geometry of Cu^{II} is closest to a seesaw conformation. The crystal structures of the complexes are built with a variety of supramolecular interactions, including the synthons N–H···X (X = N and O), which are critically discussed. The IR spectra of the compounds are discussed in terms of the coordination modes of the pseudohalido ligands. The magnetic properties of **1** and **2** have also been studied in the temperature and field ranges of 1.8–300 K and 0–50 kOe, respectively. Complex **1** exhibits both ferromagnetic and antiferromagnetic $Cu^{II}\cdots Cu^{II}$ exchange interactions propagated through the two different end-on bi-azido bridges, whereas the exchange interactions are negligible (if any) in the 2D polymer **2** as a consequence of the μ-1,5 ligation mode of the dicyanamido ligand and the resultant long $Cu^{II}\cdots Cu^{II}$ distances.

Received 12th June 2025,
Accepted 18th August 2025

DOI: 10.1039/d5dt01389e

rsc.li/dalton

Introduction

Linear pseudohalide ions such as N_3^-, NCO^-, and NCS^-, along with the larger bent dicyanamide ion, $N(CN)_2^-$, have been used as ligands in synthetic inorganic chemistry, due to their ability to coordinate with transition metal ions in various ways. For this reason, they are often named 'schizophrenics of coordination chemistry'.[1] When combined with ancillary terminal organic ligands, they facilitate the synthesis of compounds with interesting architectures and topologies.[2] This approach enables the construction of polynuclear complexes and coordination polymers with diverse properties, structures and topologies. This class of materials holds significant potential in crystal engineering, with applications in molecular sensors,[3–5] microporous materials for gas adsorption and storage,[6] electrical conductivity,[7,8] nonlinear optical activity,[9,10] catalysis,[11,12] *etc*. Bridging pseudohalides can efficiently transmit magnetic interactions between paramagnetic metal centres. As a result, pseudohalides play a crucial role in molecular magnetic systems, spanning single-molecule magnets (SMMs),[13] single-chain magnets (SCMs),[14] higher-dimensional magnetic materials,[15] and multifunctional systems such as photoactive and porous magnets.[16,17]

The N_3^- ion is one of the most common bridging ligands among pseudohalides, widely used in the synthesis of metal clusters and coordination polymers, where it imparts intri-

[a]*University of Patras, Department of Chemistry, 26504 Patras, Greece. E-mail: nastopoulos@upatras.gr, perlepes@upatras.gr*
[b]*University of Cyprus, Department of Chemistry, 1678 Nicosia, Cyprus*
[c]*Clark University, Carlson School of Chemistry and Biochemistry, Worcester, MA 01610, USA. E-mail: MTurnbull@clarku.edu*

guing magnetic and topological properties. It can act as either a terminal or a bridging ligand.[1,2,18–22] The crystallographically verified coordination modes of the azido ligand are illustrated in Scheme 1. When functioning as a monoatomic bridging ligand, the azide ion can link up to four metal ions *via* end-on (EO) coordination.[1] If both terminal nitrogen atoms participate in bonding, it acts as a bidentate bridging ligand, linking at least two metal centers through an end-to-end (EE) coordination mode. A combination of these two modes enables azide to bridge up to six metal ions. In some cases, a single compound may contain azido ligands adopting two or even three different coordination modes. It has been observed that the most common coordination mode of N_3^- in metal clusters is EO.[2,18] In 1D, 2D, and 3D coordination polymers, the EE mode predominates, sometimes alternating with EO or forming mixed EE/EO networks.[2,18,19] Coordination polymers exclusively featuring EO-bridged azides are rare. Due to the comparable stability of EO and EE coordination modes, steric hindrance is usually the key factor determining whether a complex adopts EO, EE, or a mixed EE/EO mode. The azide ion is widely used as a bridging ligand in the field of molecular magnetism, as its various coordination modes and the diverse exchange interactions it promotes lead to a range of magnetic behaviors.[2,18,19] These include ferromagnetism, antiferromagnetism, ferrimagnetism, canted weak ferromagnetism, spin-flop transitions, single-molecule magnetism (SMM), and single-chain magnetism (SCM). Literature studies indicate

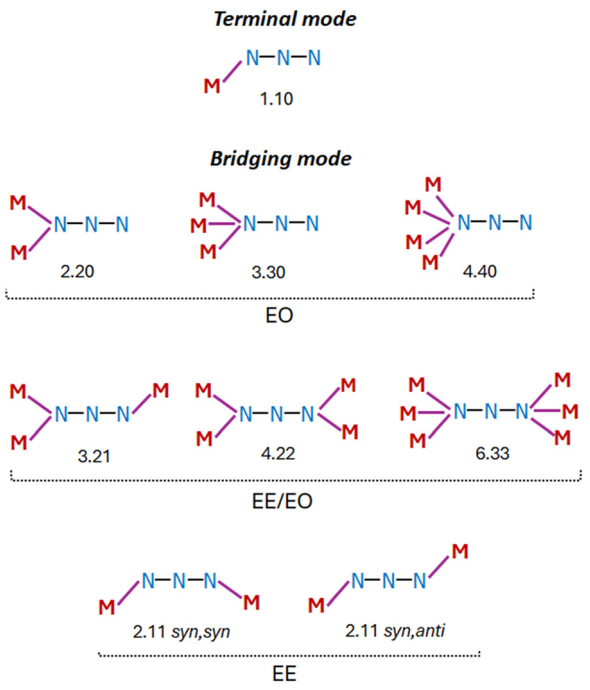

Scheme 1 The crystallographically verified coordination modes of the azido ligand in coordination chemistry with their corresponding Harris notation. Since the electronic structure within the azido ligand has not been studied in every case in detail, the bonds between the nitrogen atoms are drawn as single (which is certainly not the case).

that the end-on (EO) coordination mode typically favors ferromagnetic interactions, potentially leading to a high-spin ground state.[2,18–21] In contrast, the end-to-end (EE) mode generally promotes antiferromagnetic interactions.[2,18,21] However, the coordination mode alone is not the sole determining factor of magnetic coupling.

The relatively larger dicyanamide ion, $N(CN)_2^-$, is a flexible ligand that, in combination with transition metals, can form a wide range of compounds with diverse architectures and topologies. The dicyanamide ion has three potential donor sites and can act as either a terminal or a bridging ligand.[23–25] In polynuclear complexes, $N(CN)_2^-$ exhibits various coordination modes, binding to metal centers through the nitrogen atoms of the terminal nitrile groups, the central amido nitrogen, or both, functioning as a tridentate ligand. Consequently, dicyanamide can form coordination bonds with one to five metal ions. The coordination modes of dicyanamide, as revealed by X-ray crystallography, are illustrated in Scheme 2. These versatile binding properties enable dicyanamide to form 1D, 2D, and 3D structures, which may also exhibit interesting magnetic properties.[23–28]

Transition metal complexes with the cyanate ion (NCO^-) are of particular interest due to its ambidentate nature, allowing it to coordinate to metal ions either as a terminal or a bridging ligand through its nitrogen or oxygen atom, or both.[1,13,29–34] However, the number of polynuclear and polymeric complexes incorporating the cyanate ion is significantly smaller compared to those involving other pseudohalides. In most complexes, bonding occurs preferentially through the nitrogen atom. The N-site of NCO^- lies at the boundary between hard and soft Lewis bases (HSAB), allowing it to bind to a wide range of metal ions. In contrast, the hard O-site has a stronger affinity for hard metal ions, although this preference can be influenced by the nature of other ligands and the stereochemical environment they impose. When NCO^- acts as a monodentate ligand, it forms mononuclear complexes. However, as a bridging ligand, it can link metal centers *via* either end-on (EO) coordination modes or an end-to-end (EE) mode, as illustrated in Scheme 3.[1,13,29–34]

In recent years, we have studied a series of mononuclear complexes, primarily of the type $MX_2(HL)_2$ or $[M(HL)_4]X_2$ [M = Co^{2+}, Ni^{2+}, Cu^{2+} or Zn^{2+}; X = Cl^-, Br^-, I^-, NO_3^- or ClO_4^-; HL = 4,5-diphenylimidazole], to explore their assembly patterns, with a particular focus on both strong and weak intermolecular interactions.[35–38] This work has been recently extended to 5-phenylimidazole.[39,40] Imidazole and its derivatives[41,42] are, among others, particularly interesting ligands in bioinorganic[43,44] and metallosupramolecular[45–47] chemistry. The monodentate HL ligand employed in this work (Scheme S1) coordinates to the metal ion *via* its pyridine-type N3 atom and contains a H-bond donor (the pyrrolic-type N1 atom), enabling the formation of motifs that may drive molecular self-assembly. Additionally, it supports π···π stacking interactions through its phenyl rings and the five-membered heterocyclic ring. There has been relatively little work on the coordination chemistry of heavily substituted imidazoles and,

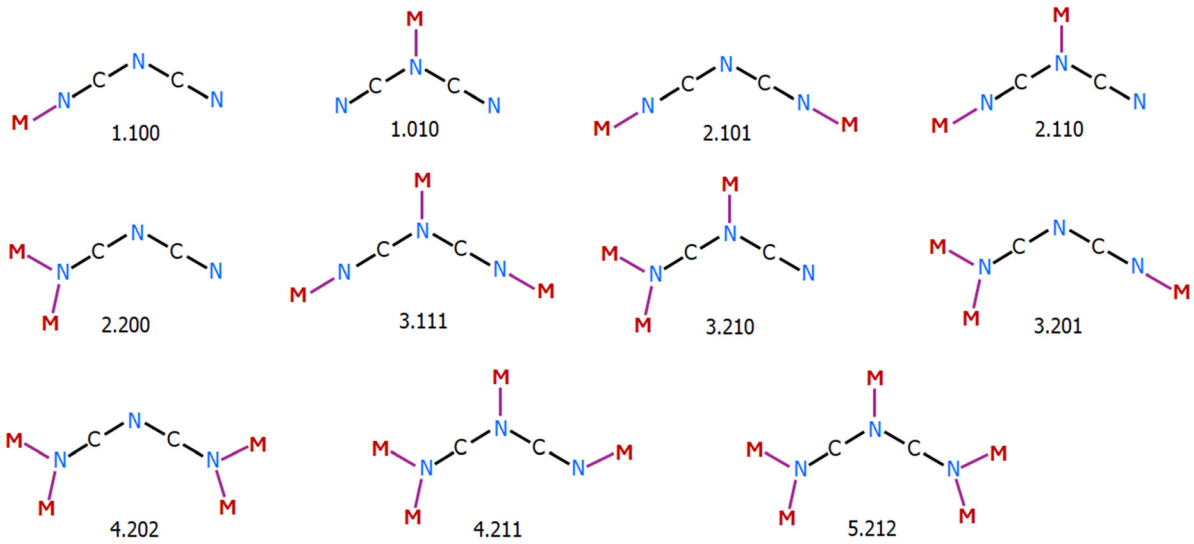

Scheme 2 The crystallographically verified coordination modes of the dicyanamido ligand in coordination chemistry with their corresponding Harris notation. Since the electronic structure within the dicyanamido ligand is not known exactly in every case, the carbon–nitrogen bonds are drawn as single (which is certainly not the case).

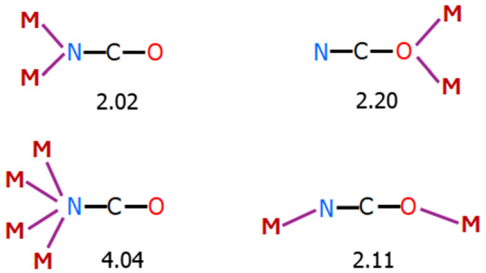

Scheme 3 Some bridging modes for the cyanato ligand observed in the literature with their corresponding Harris notation. Since the electronic structure within the cyanato ligand is not known exactly in every case, the nitrogen–carbon and carbon–oxygen bonds are drawn as single (which is certainly not the case).

in particular, about HL.[35–38,48–50] The X ions in these complexes coordinate terminally as either monodentate or bidentate ligands, thereby excluding the possibility of forming coordination polymers. Given the variation in their size and shapes, their influence on the metal's coordination geometry (when coordinated) or their spatial role in packing organization (when serving as counterions) has also been examined by our group.

In this context, it appeared interesting to explore the replacement of the halide ions with larger pseudohalides N_3^-, $N(CN)_2^-$, NCO^- and SCN^- in combination with 4,5-diphenylimidazole as an ancillary ligand in order to investigate their impact on the molecular and supramolecular organization, as well as the properties of the resulting complexes and coordination polymers. As reported, pseudohalides, when combined with other organic ligands and 3d metals, can promote the synthesis of compounds often exhibiting diverse architectures, topologies, and properties, making them a compelling area of study.

Copper(II) was selected as the metal for this study due to its versatile coordination numbers and geometries. Due to its $3d^9$ configuration, square planar or distorted tetrahedral (4-coordinate), square pyramidal or trigonal bipyramidal (5-coordinate), as well as distorted octahedral (6-coordinate) geometries dominate the coordination chemistry of copper(II). Additionally, the presence of one unpaired electron on this metal ion makes the interpretation of the magnetic properties of copper(II) complexes more straightforward compared to those of other 1st-row transition metal complexes.[51,52]

We report herein the results of the amalgamation of the above mentioned topics. Two coordination polymers, $\{[Cu(N_3)_2(HL)]\}_n$ (**1**) and $\{[Cu\{N(CN)_2\}_2(HL)]\cdot Me_2CO\}_n$ (**2**·Me_2CO), together with the mononuclear complex $[Cu(NCO)_2(HL)_2]\cdot$MeCN (**3**·MeCN), have been obtained and structurally/spectroscopically characterized, exploring the reaction system Cu^{II}/HL/pseudohalide; the magnetic properties of the polymeric complexes have also been studied. One synthetic or crystallization parameter at a time was varied during each set of experiments so as to assess its relative effect on the product identity.

Experimental

Materials and instruments

All reagents, solvents and starting materials were reagent grade, purchased from standard suppliers and used as received. All manipulations were performed under aerobic conditions. Microanalyses (C, H, and N) were performed by the University of Patras microanalytical service. IR spectra (4000–400 cm^{-1}) were recorded using a Perkin-Elmer PC 16 FT-IR spectrometer with the samples prepared as KBr pellets. For magnetic studies, samples of compounds **1** and **2** were

powdered and mounted in gelatine capsules placed in clear plastic straws. Magnetization data, as a function of field (0–50 kOe), were collected at 1.8 K for compounds **1** and **2** employing a Quantum Design MPMS-5 SQUID magnetometer. Several data points were recollected as the field was returned to zero; no hysteresis was observed. Data were then collected in a 1 kOe field as a function of temperature from 1.8 to 310 K. Measurements were corrected for the diamagnetism of the constituent atoms as estimated from Pascal's constants, the temperature independent paramagnetism of the Cu(II) ion and the gelatine capsule and straw (measured independently).

Safety note: Azido and dicyanamido compounds and perchlorate salts are potentially explosive; such compounds should be synthesized and used in small quantities and treated with utmost care at all times.

Preparation of complexes

Synthesis of $\{[Cu(N_3)_2(HL)]\}_n$ (1). A solution of $Cu(ClO_4)_2{\cdot}6H_2O$ (0.10 mmol, 0.037 g) and 4,5-diphenylimidazole (0.25 mmol, 0.055 g) in 5 mL of DMF and a solution of NaN_3 (0.20 mmol, 0.013 g) in 20 mL of methanol were prepared. The two solutions were mixed and then stirred for 10 minutes. The resultant brown solution was filtered, and the filtrate was stored in a closed vial at room temperature. Dark red/brown plate-like crystals of **1**, suitable for X-ray diffraction, were obtained after five days. They were collected by filtration, washed with Et_2O (2 × 5 mL) and dried *in vacuo*. Yield *ca.* 65% (based on the metal). Anal. calcd for $C_{15}H_{12}N_8Cu$ (found values in parentheses): C 48.98 (49.40), H 3.29 (3.11), N 30.46 (30.24)%. IR bands (KBr, cm^{-1}): 3446wb, 3194mb, 3050w, 2883w, 2074s, 2050s, 1587w, 1510m, 1486m, 1460w, 1442m, 1382w, 1344w, 1290m, 1278sh, 1190w, 1155w, 1136m, 1072m, 978m, 764m, 724w, 696m, 650m, 574w, 508w.

Synthesis of $\{[Cu\{N(CN)_2\}_2(HL)]{\cdot}Me_2CO\}_n$ (2·Me$_2$CO). 4,5-diphenylimidazole (0.20 mmol, 0.044 g) was dissolved in 25 mL of Me_2CO under stirring and mild heating (50 °C). To this solution, solid $Cu(ClO_4)_2{\cdot}6H_2O$ (0.10 mmol, 0.037 g) was added, resulting in a clear yellow/green solution. Subsequently, $Na\{N(CN)_2\}$ (0.20 mmol, 0.018 g) was added, leading to the formation of a dark turbid yellow-green slurry. This slurry was stirred for 10 minutes, the resultant olive-coloured solution was filtered and the filtrate was layered with Et_2O (5 mL/5 mL). Green prismatic crystals of **2**·Me_2CO, suitable for X-ray diffraction, were obtained after seven days. They were collected by filtration, washed with Et_2O (2 × 5 mL) and dried *in vacuo*. Yield *ca.* 60% (based on the metal). Anal. calcd for $C_{19}H_{12}N_8Cu$ (*i.e.*, **2**) [found values in parentheses]: C 54.87 (55.22), H 2.91 (2.80), N 26.94 (26.69)%. IR bands (KBr, cm^{-1}): 3446mb, 3230mb, 3136w, 3048w, 2923w, 2300w, 2240sh, 2222m, 2194s, 1702s, 1654w, 1604w, 1542w, 1518m, 1490w, 1458w, 1398m, 1364s, 1236w, 1138w, 1074w, 976w, 920w, 776sh, 764m, 706w, 680w, 646m, 576w, 504m.

Synthesis of $[Cu(NCO)_2(HL)_2]{\cdot}MeCN$ (3·MeCN). 4,5-diphenylimidazole (0.25 mmol, 0.055 g) was dissolved in 25 mL of MeCN under stirring and mild heating (40 °C). To this solution, solid $Cu(ClO_4)_2{\cdot}6H_2O$ (0.10 mmol, 0.037 g) was added, resulting in a clear crimson solution. Subsequently, NaNCO (0.20 mmol, 0.013 g) was added, leading to the formation of a turbid black-yellow slurry. This slurry was stirred for 15 minutes, the resultant dark green solution was then filtered and the green filtrate was layered with a mixture of Et_2O/*n*-hexane (5 mL/5 mL). Green prismatic crystals of **3**·MeCN, suitable for X-ray diffraction, were obtained after one day. They were collected by filtration, washed with Et_2O (2 × 5 mL) and dried *in vacuo*. Yield *ca.* 60% (based on the metal). Anal. calcd for $C_{32}H_{24}N_6O_2Cu$ (*i.e.*, **3**) [found values in parentheses]: C 65.35 (65.59), H 4.11 (4.18), N 14.29 (13.99)%. IR bands (KBr, cm^{-1}): 3446mb, 3196wb, 3058w, 2922w, 2216s, 2170sh, 1604w, 1560w, 1510m, 1486m, 1468w, 1444m, 1382w, 1332m, 1294w, 1276w, 1130w, 1072m, 1026w, 976m, 912w, 764m, 724w, 696s, 648m, 616w, 578w, 499w.

X-ray crystallography

A suitable single crystal of each of the three compounds was selected, coated with Paratone-N oil, and mounted in cryo-loops at the end of a copper pin. Diffraction data were collected using the ω-scan technique on a Rigaku Oxford Diffraction SuperNova diffractometer under a stream of nitrogen gas at 100(2) K; Cu Kα radiation (λ = 1.5418 Å) was used for compounds **1** and **2**·Me_2CO, while Mo Kα radiation (λ = 0.7107 Å) was used for compound **3**·MeCN. Table 1 shows the summary of crystallographic data. Data were collected and processed using CRYSALIS CCD and RED software,[53] respectively; the reflection intensities were corrected for absorption using the multiscan method. The structures were solved using classical direct methods (SIR92,[54] Semi-Invariants Representation), the dual-space algorithm with SHELXT,[55] or the charge flipping algorithm (Superflip[56,57]). The structural models were then refined by full-matrix least-squares on F^2 with SHELXL-2019/3.[58] All non-H atoms were refined anisotropically; carbon-bound H atoms were introduced at calculated positions and allowed to ride on their carrier atoms (riding model). All imidazole H atoms on the pyrrolic-type N1 atom of the ligands were located in difference Fourier maps and refined isotropically applying soft distance restraints. Considerable disorder has been observed in the crystal structure of compound **3**·MeCN. One of the phenyl rings in the HL ligand exhibits positional disorder, which was treated by applying a two-part disorder model with a 57 : 43 domain ratio. Additionally, the MeCN solvent molecule is orientationally disordered (50 : 50) about a two-fold axis running parallel to the *b* axis of the unit cell. Appropriate restraints were applied during refinement to ensure a chemically reasonable geometry for each disordered component.

Geometric/crystallographic calculations were carried out using PLATON,[59] OLEX2[60] and WINGX[61] packages; molecular/packing graphics were prepared using MERCURY.[62]

Results and discussion

Synthetic comments

A variety of reactions were studied with the aim of preparing the largest possible number of compounds (discrete complexes

Table 1 Crystallographic data for compounds $\{[Cu(N_3)_2(HL)]\}_n$ (**1**), $\{[Cu\{N(CN)_2\}_2(HL)]\cdot Me_2CO\}_n$ (**2**·Me_2CO) and $[Cu(NCO)_2(HL)_2]\cdot MeCN$ (**3**·MeCN)

Compound reference	**1**	**2**·Me_2CO	**3**·MeCN
Chemical formula	$C_{15}H_{12}CuN_8$	$C_{19}H_{12}CuN_8\cdot C_3H_6O$	$C_{32}H_{24}CuN_6O_2\cdot C_2H_3N$
Formula mass g^{-1} mol^{-1}	367.87	473.98	629.16
Crystal system	Monoclinic	Monoclinic	Orthorhombic
Space group	$P2_1/n$	$P2_1/n$	*Pbcn*
a/Å	9.2102(3)	7.7400(2)	17.0660(7)
b/Å	5.5759(2)	11.7233(3)	12.7219(4)
c/Å	30.9154(9)	23.8510(5)	13.6879(6)
α/°	90	90	90
β/°	92.515(3)	94.612(2)	90
γ/°	90	90	90
Unit cell volume $Å^{-3}$	1586.14(9)	2157.19(9)	2971.8(2)
Z, *Z*′	4, 1	4, 1	4, 0.5
Temperature/K	100(2)	100(2)	100(2)
Radiation type, *μ*/mm^{-1}	CuKα, 2.071	CuKα, 1.696	MoKα, 0.779
No. of reflections measured	5882	13 654	24 688
No. of independent reflections	3022 [R_{int} = 0.0216]	4159 [R_{int} = 0.0318]	2759 [R_{int} = 0.0439]
Data/restraints/parameters	3022/0/220	4159/1/294	2759/147/247
Final R_1 values ($I > 2\sigma(I)$)	0.0306	0.0308	0.0666
Final w$R(F^2)$ values ($I > 2\sigma(I)$)	0.0790	0.0792	0.1548
Final R_1 values (all data)	0.0373	0.0366	0.0719
Final w$R(F^2)$ values (all data)	0.0832	0.0834	0.1574
Goodness of fit on F^2	1.033	1.026	1.231
$\Delta\rho_{max}$, $\Delta\rho_{min}$/e $Å^{-3}$	0.376, −0.500	0.307, −0.369	1.039, −1.773
CCDC number	2456934	2456935	2456936

or polymers) by exploring the Cu^{II}/HL/pseudohalide system (HL = 4,5-diphenylimidazole; pseudohalide = N_3^-, $N(CN)_2^-$, NCO^-, and SCN^-). Our trials included differing reactant ratios and concentrations, solvents, crystallization conditions and temperatures. Cu(II) is air stable, and the synthetic work was thus performed under aerobic conditions under the normal laboratory atmosphere. The reagents utilized in the experiments as sources for the respective ions in the reaction scheme involved $Cu(ClO_4)_2\cdot 6H_2O$ for copper(II) ions; NaN_3 and $(CH_3)_3SiN_3$ for azide ions; $Na\{N(CN)_2\}$ for dicyanamide ions; NaNCO for cyanate ions; and NH_4SCN for thiocyanate ions. Two coordination polymers have been obtained, $\{[Cu(N_3)_2(HL)]\}_n$ (**1**) and $\{[Cu\{N(CN)_2\}_2(HL)]\cdot Me_2CO\}_n$ (**2**·Me_2CO). Efforts to isolate an analogous coordination polymer using cyanates resulted in the formation of the mononuclear complex $[Cu(NCO)_2(HL)_2]\cdot MeCN$ (**3**·MeCN). Compounds were obtained by reactions with a Cu^{II} : HL : pseudohalide ratio of 1 : 2.5 : 2 for **1** and **3**·MeCN and 1 : 2 : 2 for **2**·Me_2CO. Despite our efforts, no crystalline thiocyanato solids have been obtained yet. The formation of the complexes can be summarized by eqn (1)–(3):

$$n\mathrm{Cu(ClO_4)_2\cdot 6H_2O} + 2n\mathrm{NaN_3} + n\mathrm{HL} \xrightarrow{\mathrm{DMF/MeOH}} \underset{\mathbf{1}}{\{[\mathrm{Cu(N_3)_2(HL)}]\}_n} + 2n\mathrm{NaClO_4} + 6n\mathrm{H_2O} \quad (1)$$

$$n\mathrm{Cu(ClO_4)_2\cdot 6H_2O} + 2n\mathrm{Na\{N(CN)_2\}} + n\mathrm{HL} + n\mathrm{Me_2CO} \xrightarrow[\mathrm{T}]{\mathrm{Me_2CO}} \underset{\mathbf{2\cdot Me_2CO}}{\{[\mathrm{Cu\{N(CN)_2\}_2(HL)}]\cdot \mathrm{Me_2CO}\}_n} + 2n\mathrm{NaClO_4} + 6n\mathrm{H_2O} \quad (2)$$

$$\mathrm{Cu(ClO_4)_2\cdot 6H_2O} + 2\mathrm{NaNCO} + 2\mathrm{HL} + \mathrm{MeCN} \xrightarrow[\mathrm{T}]{\mathrm{MeCN}} \underset{\mathbf{3\cdot MeCN}}{[\mathrm{Cu(NCO)_2(HL)_2}]\cdot \mathrm{MeCN}} + 2\mathrm{NaClO_4} + 6\mathrm{H_2O} \quad (3)$$

It should be mentioned that complexes **1**–**3** are the only products from their corresponding reaction mixtures irrespective of the Cu^{II} : HL reaction ratio. Thus, a large excess of HL (*e.g.*, Cu^{II} : HL = 1 : 4) resulted again in the polymeric 1 : 1 complexes **1** and **2**, and thus mononuclear complexes $[CuX_2(HL)_2]$, where X = N_3 and $N(CN)_2$, could not be isolated. An excess of metal (*e.g.*, Cu^{II} : HL = 1 : 1) led again to the mononuclear complex **3**, and the anticipated $\{[Cu(NCO)_2(HL)]\}_n$ complex could not be prepared.

All crystalline products were characterized by IR spectroscopy, microanalyses and single-crystal X-ray diffraction; the magnetic properties of the polymeric compounds were also studied.

Description of the structures

For consistency in discussion and molecular comparison, the same numbering scheme has been assigned to the HL ligand atoms across all three compounds presented herein. Selected interatomic distances and angles for all compounds are provided in Table S1. Details of H-bonding, C–H···π and π···π interactions are given in Tables S2–S4, respectively. Various structural plots are shown in Fig. 1–5 and S1–S4.

Compound **1** crystallizes as a 1D polymer in the monoclinic space group $P2_1/n$. The asymmetric unit comprises one Cu^{II} ion, two azido groups, and one 4,5-diphenylimidazole molecule (Fig. S1). The two azido groups (N4–N5–N6 and N7–N8–N9) act as monoatomic bridging ligands in an end-on (μ-1,1 or 2.20) mode connecting two metal centres through the N4 and N7 atoms, respectively. Due to crystallographic symmetry, each

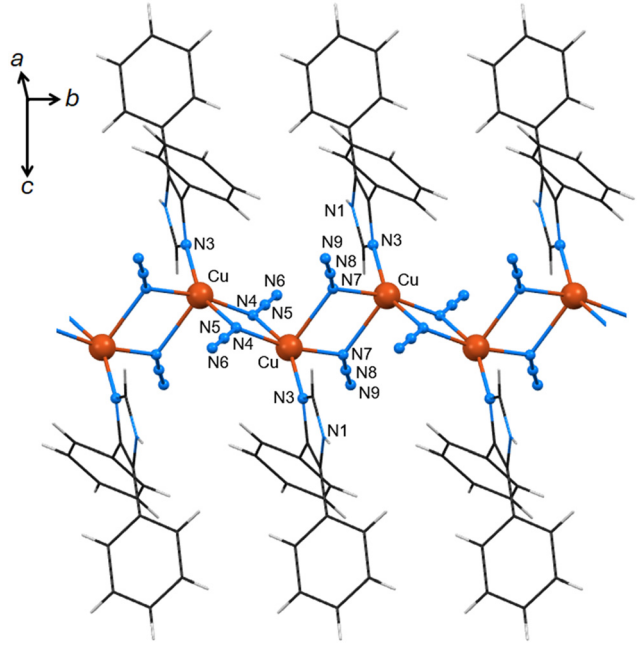

Fig. 1 Perspective view of a fraction of the chain of $\{[Cu(N_3)_2(HL)]\}_n$ (**1**). The azido ligands adopt the end-on (μ-1,1 or 2.20) bridging mode, connecting Cu^{II} centers in a linear arrangement to form a 1D coordination polymer extending along the *b*-axis. Atoms generated by symmetry operations have been included but have been labelled identically to the asymmetric unit.

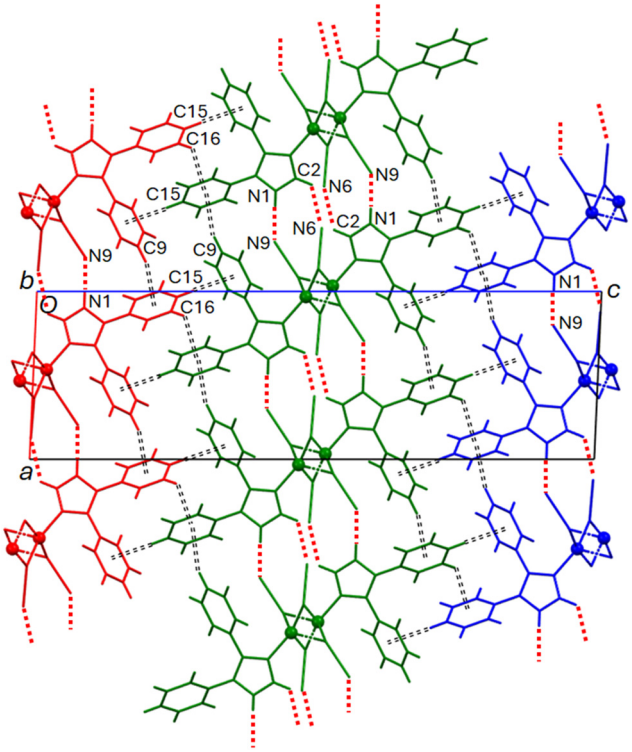

Fig. 2 Section of the 3D architecture of the polymer $\{[Cu(N_3)_2(HL)]\}_n$ (**1**). Three layers (marked in red, green and blue) parallel to the *ab* plane are drawn. Within each layer, the chains (oriented parallel to the *b* axis) are interconnected by strong N1–H1···N9 hydrogen bonds (dotted red lines) and weak C–H···N interactions (C2–H2···N6). Additionally, weak C–H···π interactions (black double dashed lines) between the chains of each layer, as well as between parallel layers, contribute to the 3D self-organization of the polymer. Cu^{II} atoms are drawn as small spheres. Atoms generated by symmetry operations have been included but have been labelled identically to the asymmetric unit.

Cu^{II} centre is ultimately coordinated by four azido groups, with its coordination sphere completed by the pyridine-type N3 atom of a 4,5-diphenylimidazole ligand. As a result, the metal ions adopt a five-coordinate (CuN_5) environment. According to the angular structural parameter τ_5,[63] the Cu^{II} coordination geometry is a distorted square pyramid, where the N7 symmetry-related atom $(1 - x, 1 - y, -z)$, located at a distance of 2.330(2) Å from copper(II), occupies the apical position (Fig. S2). The τ_5 value is 0.25, where $\tau_5 = 0$ corresponds to an ideal square pyramidal geometry and $\tau_5 = 1$ corresponds to an ideal trigonal bipyramidal geometry. The Cu–N bond lengths range from 1.968(2) to 2.330(2) Å. The bond length of the apical nitrogen atom is the largest, as expected. The N–N bond lengths in the two azido ligands, corresponding to the coordinated and central nitrogen atoms (*i.e.*, N4–N5 = 1.215 Å and N7–N8 = 1.198 Å), are longer than those between the central and non-coordinated terminal nitrogen atoms (*i.e.*, N5–N6 = 1.133 Å and N8–N9 = 1.156 Å, respectively). This elongation is attributed to the 'loss' of electron density at the two bridging nitrogen atoms. The N–N–N bond angles of the two nearly linear azido ligands are 179.2(2)° and 176.7(2)° for N4–N5–N6 and N7–N8–N9, respectively.

The 1D polymer $\{[Cu(N_3)_2(HL)]\}_n$ is made up of undulating Cu-azido chains, with the coordinated HL ligands extending from both sides of the chains (Fig. 1). These chains extend parallel to the *b* axis of the unit cell, with Cu···Cu distances of 3.093(1) and 3.317(1) Å between consecutive Cu^{II} atoms along the chain. At a supramolecular level, these parallel chains are linked by strong hydrogen bonds (synthons) of the type $N1_{imidazole}$–$H1\cdots N9_{azide}$ [N1···N9 = 2.923(2) Å], together with weak C–H···N_{azide} interactions, forming layers parallel to the *ab* plane (Fig. 2 and Table S2). These interactions contribute to the self-assembly and stabilization of the crystal structure. Finally, the three-dimensional structure is further stabilized by weak C–H···π interactions between the chains within each layer, as well as between adjacent layers (Fig. 2 and Table S3).

Compound **2**·Me_2CO, containing the dicyanamido ligand, crystallizes in the monoclinic space group $P2_1/n$. The asymmetric unit consists of a Cu^{II} atom coordinated with two dicyanamide ions and one molecule of 4,5-diphenylimidazole (HL). The structure also incorporates an acetone molecule as a consequence of the crystallization process (Fig. S3). The dicyanamide ions act as bridging ligands through their nitrogen atoms N4 and N6, as well as atoms N7 and N9 of the nitrile groups (coordination mode: end-to-end, 2.101 or μ-1,5). This arrangement forms a 2D polymeric structure parallel to the *ab* plane of the unit cell, consisting of four-membered metal rings interconnected by four dicyanamide bridges (Fig. 3, left).

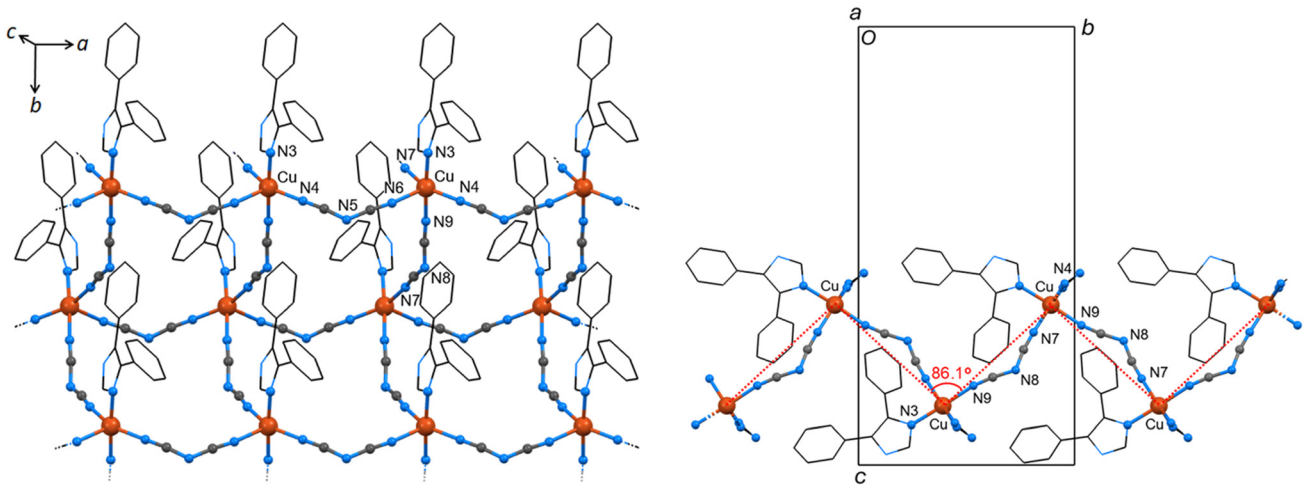

Fig. 3 (Left) Part of the 2D polymer of **2**·Me_2CO parallel to the *ab* plane of the unit cell. (Right) Projection of the structure of **2**·Me_2CO along the *a* axis. The planes defined by the four Cu^{II} atoms of each ring of the structure are indicated by red dotted lines. Atoms generated by symmetry operations have been included but have been labelled identically to the asymmetric unit. The lattice acetone molecule is not shown.

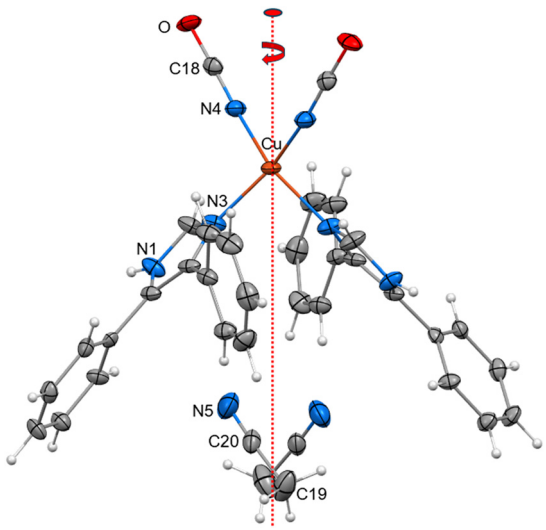

Fig. 4 The molecular structure of compound **3**·MeCN. The acetonitrile solvent molecule is orientationally disordered (50 : 50) about a two-fold symmetry axis passing through the Cu^{II} atom. Only the major occupancy orientation of the positionally disordered phenyl ring in the HL ligand is shown. Thermal ellipsoids are drawn at the 50% probability level, with selected atoms labeled. H atoms are represented as fixed-size spheres.

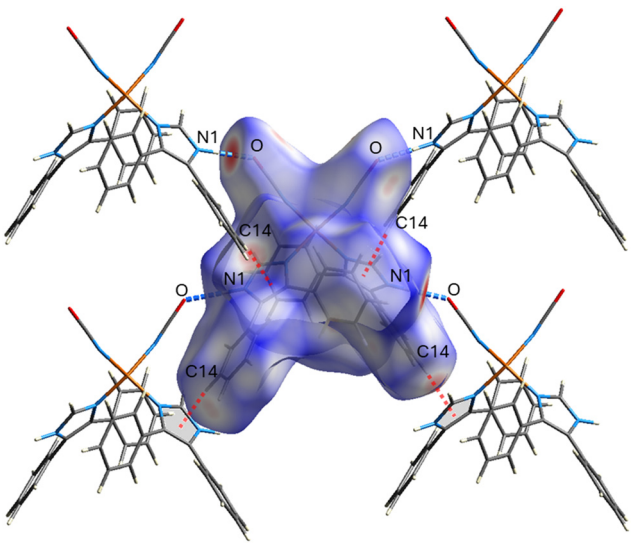

Fig. 5 Hirshfeld surface analysis of compound **3**·MeCN mapped over the d_{norm} function. d_{norm} is a function of distances to the surface from nuclei inside and outside the Hirshfeld surface, relative to their respective van der Waals radii. All the red spots on the Hirshfeld surface represent the interactions, whereas the blue ones indicate the areas without close contacts. The strong N–H···O interactions are shown as blue dashed lines and the C–H···π contacts as red dashed lines.

The coordination sphere of the metal ions is completed by the pyridine-like nitrogen atom (N3) of the 4,5-diphenylimidazole ligand (HL). The five-coordinate Cu^{II} ion (with a τ_5 index value of 0.51) adopts a geometry intermediate between square pyramidal (τ_5 = 0) and trigonal bipyramidal (τ_5 = 1). When viewed along the *a* axis (Fig. 3, right), the 2D structure is best described as a corrugated surface parallel to the *ab* plane, with the four Cu^{II} ions of each ring positioned at the intersection of the planes of the corrugated surface. The dihedral angle between adjacent planes of this surface is 86.1(1)°. The Cu···Cu distances within the rings are 7.740(1) Å and 8.227(1) Å. Weak interactions, such as π···π stacking between aromatic rings of parallel layers and C–H···$N_{dicyanamide}$ interactions, contribute to the self-assembly of the polymeric structure. Finally, the N1–H1 donor group does not engage in any H-bonding within the complex, presumably due to steric hindrance. Instead, it forms a hydrogen bond with the oxygen atom of an acetone molecule [$N1_{imidazole}\cdots O_{acetone}$ = 2.848(2) Å], which accounts for the incorporation of this crystallization molecule into the crystal lattice (Tables S2 and S4).

The crystal structure of compound $[Cu(NCO)_2(HL)_2]\cdot MeCN$ (**3**·MeCN) is orthorhombic with the space group *Pbcn*. The mononuclear complex exhibits molecular symmetry, with a two-fold rotation axis passing through its Cu^{II} centre (Fig. 4). Additionally, the MeCN solvent molecules exhibit orientational disorder, occupying two symmetrically equivalent positions around the two-fold axis in a 50 : 50 ratio. The metal centre of the complex is bonded to two HL ligands *via* the pyridine-type nitrogen atoms of their imidazole rings, along with two terminal cyanate ions coordinated through their nitrogen atoms (isocyanato ligands). According to the τ_4 metrical parameter proposed by Yang, Powell, and Houser[64] for assessing the geometry of 4-coordinate metal ions, the coordination geometry of Cu^{II} is closest to a seesaw configuration (τ_4 = 0.38). This parameter ranges from 1 for ideal tetrahedral (T_d) geometry to 0.85 for trigonal pyramidal (C_{3v}) and 0 for square planar (D_{4h}) geometry. The seesaw geometry, with an ideal C_{2v} (mm2) symmetry, lies between trigonal pyramidal and square planar structures. However, in this case, the geometry is distorted due to steric restraints imposed by the bulky 4,5-diphenylimidazole ligands. As a result, only the two-fold axis is retained, allowing the two ligands to adopt a favourable 'antiparallel' arrangement with their aromatic rings oriented in opposite directions (Fig. 4). The NCO^- ion is nearly linear with an N–C–O angle of 177.8(6)°. At the supramolecular level, strong $N1_{imidazole}$–$H1\cdots O_{NCO}$ hydrogen bonds [N1···O = 2.826(6) Å] assemble the complexes into 2D layers parallel to the *ab* plane (Fig. S4). These layers are further interconnected by a few C–H···π interactions that enhance the stability of the overall 3D architecture (Tables S2 and S3). The visualization of these interactions in the crystal structure of compound **3**·MeCN using Hirshfeld surface analysis is shown in Fig. 5. The 3D molecular Hirshfeld surface is defined by the molecule and the proximity of its nearest neighbours, effectively capturing information about all intermolecular interactions. The MeCN solvent molecules are located in channels extending along the *c* axis of the unit cell. PLATON analysis indicates that, after solvent removal, the calculated void space of the channels accounts for 10.7% of the unit cell volume (Fig. S4).

IR spectroscopy in brief

The three complexes were characterized by IR spectroscopy. The spectra exhibit the characteristic bands of the phenyl and imidazole rings of coordinated HL. The weak to medium band at *ca.* 3200 cm^{-1} is attributed to the ν(NH) vibration. The broadness and rather low wavelength of this band are both indicative of hydrogen bonding. We comment now on the bands due to the pseudohalide groups.

The spectrum of **1** exhibits two strong bands at 2074 and 2050 cm^{-1}, assigned to the asymmetric stretching mode of the monoatomic bridging azido ligands, ν_{as}(NNN).[65,66] The appearance of two bands reflects the presence of two, crystallographically independent, 2.20 azido groups in the structure. The shoulder at 1278 cm^{-1} and the weak band at 574 cm^{-1} can be tentatively assigned to the ν_s(NNN) and δ(NNN) vibrations, respectively.[65] The free dicyanamide ion in $Na\{N(CN)_2\}$ shows three sharp and medium to strong characteristic stretching bands in the 2290–2175 cm^{-1} region attributable to a ν_{as}(C–N) + ν_s(C–N) combination mode (2286 cm^{-1}) and the ν_{as}(C≡N) (2232 cm^{-1}) and ν_s(C≡N) (2179 cm^{-1}) vibrations.[24,25,65] The shift of these bands to higher wavenumbers in the spectrum of **2** (2300–2194 cm^{-1}) is characteristic of the bidentate bridging 2.101 ligation mode of $N(CN)_2^-$; monodentate coordination has been reported to have a minor effect on these features. The linear triatomic free (*i.e.*, ionic) NCO^- species belongs to the $C_{\infty v}$ point group. The three normal modes of vibration (ν_1, ν_2, and ν_3) are IR- and Raman-active. These vibrations are commonly described as unmixed group frequencies, even though this is an approximation. Thus, the pseudo-antisymmetric stretching frequency (ν_1) is referred to as the ν(C≡N) mode, the pseudo-symmetric stretching frequency (ν_3) to the ν(C–O) mode and ν_2 to the doubly degenerate deformation or bending δ(NCO) vibration.[29] The ν_1, ν_2 and ν_3 vibrations of the free cyanate ion (*i.e.*, in KNCO) appear at 2160, 630 and 1250 cm^{-1}, respectively. The corresponding modes in **3** are associated with the bands at 2216, 616 and 1276 cm^{-1}. The shift of the stretching bands to higher wavenumbers in the spectrum of the complex, compared to those in KNCO, is indicative of N-coordination.[29,65]

Magnetochemistry

Direct current (dc) magnetic susceptibility data (χ) on dried, analytically pure samples of **1** and **2** were collected in the 1.8–310 K range in an applied field of 1 kOe. Data are presented in Fig. 6, 7, S5 and S6. We describe the results using the emu convention.

The magnetization (M) as a function of field (H) plot for complex **1** at 1.8 K (Fig. S5) is featureless. The curvature shows

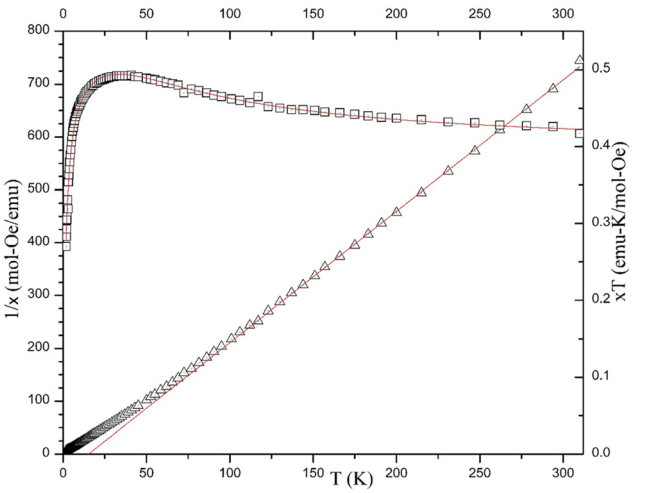

Fig. 6 Temperature dependence of $1/\chi$ (left axis) and the χT product (right axis) for an analytically pure sample of compound **1** collected in a **1** kOe field; χ is the molar magnetic susceptibility that equals M/H and T is the absolute temperature. The solid lines show the best fit to the Curie–Weiss law from 310 to 112 K for the $1/\chi$ data and the fit to the dimer model (with a Curie–Weiss correction for interdimer corrections) for the χT data.

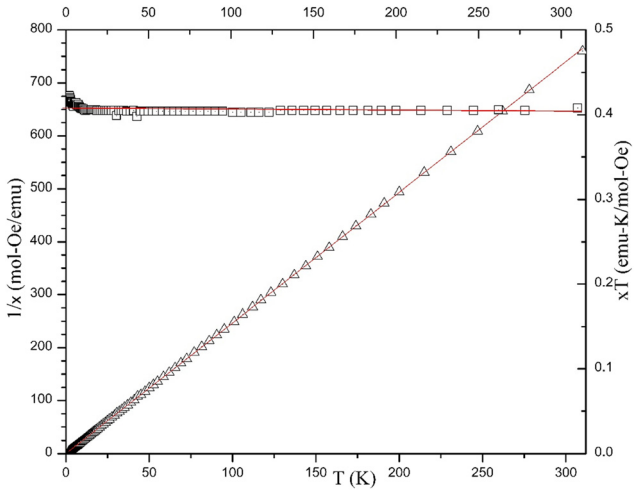

Fig. 7 Temperature dependence of $1/\chi$ (left axis) and the χT product (right axis) for an analytically pure sample of compound **2**. The solid lines show the best fit to the Curie–Weiss law from 310 to 10 K.

that it is approaching saturation near 5400 emu mol^{-1} at 50 kOe, but has not yet reached it. This is very reasonable for an $S = 1/2$ system with g slightly greater than 2.00, as is typical for Cu(II) complexes in the presence of weak antiferromagnetic interactions.

The χ as a function of T plot is interesting. The χ *versus* T data appear featureless, but the $1/\chi$ *versus* T and χT *versus* T data (Fig. 6) clearly show the presence of magnetic exchange within the system. Although linear at high temperatures, the $1/\chi$ data show a positive intercept, indicative of dominant ferromagnetic interactions, and a distinct curvature with decreasing temperature. The data were fit to the Curie–Weiss law from 310 K downward with a decreasing lower T limit until the quality of fit and the value of θ (Weiss constant) began to change significantly. This yielded a lower limit of 112 K with a Curie constant $C = 0.402(2)$ emu K mol^{-1} Oe and $\theta = +15.1(9)$ K. Decreasing the lower limit to 101 K resulted in $\theta = +14.3(10)$ K and decreasing to 95 K gave $\theta = +13.7(8)$ K. The Curie constant was stable within the error over all these temperature ranges. The steady decrease in θ as the lower temperature decreases indicates the presence of weaker antiferromagnetic exchange in addition to ferromagnetic interactions. The plot of the χT *versus* T data confirms the presence of both ferromagnetic and antiferromagnetic interactions. As T decreases, the χT product slowly increases from 0.42 to a maximum of 0.49 emu K mol^{-1} Oe at 41 K. Below this temperature, the χT product begins to decrease rapidly, reaching a value of 0.27 emu K mol^{-1} Oe at 1.8 K. An examination of the molecular structure suggests an explanation for the presence of both interactions. Although there is a single, crystallographically unique Cu^{II} atom in the molecule, there are two different biazide bridges that link these metal ions into a chain (Fig. 1). One bridge (possessing the N4 atoms) not only exhibits nearly symmetrical azido coordination [Cu–N bond lengths of 1.988(2) and 2.009(2) Å], but also connects the Cu^{II} atoms through basal–basal Cu–N bonds. In contrast, the other bridging interaction (containing the N7 atoms) is quite unsymmetrical [Cu–N bond lengths of 1.989(2) and 2.330(1) Å], since one of these bonds lies in the apical site of the square pyramidal geometry. In other words, one azido nitrogen N7 occupies a position in the basal plane of one Cu^{II} atom, while the same nitrogen occupies the apical position of the neighboring metal ion (see Table S1). The Cu–N7–Cu and Cu–N4–Cu bridging angles are quite similar [100.1(1) and 101.4(1)°, respectively] and unlikely to be the cause of such a dramatic magnetic exchange shift. Given these observations, the χT *versus* T data were fit to a ferromagnetic dimer model, with a Curie–Weiss correction for weak interdimer interactions (the solid line in Fig. 6), resulting in $C = 0.394(1)$ emu K mol^{-1} Oe, $J/K_B = 104(3)$ K and $\theta = -1.59(2)$ K. We propose[67–76] that the stronger ferromagnetic interaction occurs *via* the basal–apical bridge as is often observed and these dimeric units are then linked *via* the weaker basal–basal interaction. It has been reported that the basal–apical bis(EO)-bridged dicopper(II) units, like the $\{Cu_2(N7)_2\}$ unit in **1**, are characterized by ferromagnetic Cu$^{II}\cdots$Cu^{II} exchange interactions.[67,71] Examples are the 1D compounds $[Cu_2(EO\text{-}N_3)_2(ta)(phen)_2]$[72] (ta is the bridging terephthalato dianion) with $J/K_B = 17.8$ K and the dimeric complex $[Cu_2(EO\text{-}N_3)_2(L)_2]$[73] (L is the bidentate chelating 7-amino-4-methyl-5-aza-3-heptan-2-onato monoanion) with $J/K_B = 34.6$ K. Exceptions to this general trend are known, for example, in the dimeric complexes $[Cu_2(EO\text{-}N_3)_2Cl_2(phen)_2]$[74] (phen is 1,10-phenanthroline) and $[Cu_2(EO\text{-}N_3)_2(dpt)_2](ClO_4)_2$[75] (dpt is the tridentate chelating ligand dipropylenetriamine) with almost negligible Cu$^{II}\cdots$Cu^{II} exchange interaction. From the structural and magnetic viewpoints, the closest complex to **1** is the 1D compound $\{[Cu(N_3)_2(quin)]\}_n$[76] (quin is quinoline), which also possesses alternating basal–apical and basal–basal bi(EO) azido bridges. Similarly to **1**, this complex exhibits ferromagnetic coupling ($J/K_B = 6.6$ K) with the onset of a weak antiferromagnetic coupling at low temperatures; the smaller J constant (compared to **1**) may be due to the geometry of the Cu^{II} ion, which is intermediate between square pyramidal and trigonal bipyramidal ($\tau_5 = 0.47$ in the quinoline compound *vs.* 0.25 in **1**). The structurally similar 1D compounds $\{[Cu(EO\text{-}N_3)_2L']\}_n$, where L′ is 2,4-dimethylpyridine,[77] 2,5-dimethylpyridine,[78] and 2-chloropyridine,[79] have not been studied by dc magnetometry.

The M as a function of H plot (Fig. S6) for compound **2** increases steadily to 50 kOe where it nears saturation and reaches a value of ~5500 emu mol^{-1}, in good agreement with the expected value for a $S = 1/2$ ion with g slightly greater than 2 (~6000 emu mol^{-1}). M as a function of T was then measured in a 1000 Oe field from 1.8 to 310 K. The χ value rises monotonically with decreasing T, reaching a value of 1.32×10^{-3} emu mol^{-1} Oe at 310 K. The data, plotted as χT *versus* T and $1/\chi$ *versus* T, are shown in Fig. 7. The $1/\chi$ *versus* T plot is linear over the entire temperature range and was fit to the Curie–Weiss law to yield a Curie constant C of 0.405(1) emu K mol^{-1} Oe and a Weiss constant θ of virtually zero [−0.04(4) K], indicating the absence of magnetic exchange interactions over the whole

temperature range. The χT *versus* T data were also fit to the Curie–Weiss law with the same result within experimental error. The small upturn in this plot at the lowest temperatures could signal extremely weak ferromagnetic interactions but is much more likely due to a small error in the background measurement. The negligible (if any) $Cu^{II}\cdots Cu^{II}$ exchange interactions are reasonable, given the 2.101 (μ-1,5) coordination mode of $N(CN)_2^-$ and the resultant very long (>7.5 Å) copper(II)–copper(II) distances (*vide supra*).[23]

Conclusions and perspectives

The chemical message of this work is the ability of N_3^- and $N(CN)_2^-$ to form coordination polymers of copper(II) in the presence of 4,5-diphenylimidazole (HL). The complexes have interesting molecular and supramolecular structures, and the dimensionality (1D *versus* 2D) of the product depends on the pseudohalide ligand used. In addition, the azido complex exhibits both ferromagnetic and antiferromagnetic $Cu^{II}\cdots Cu^{II}$ exchange interactions. Efforts to isolate analogous coordination polymers using NCO^- were in vain, illustrating the greater preference of this ion for terminal coordination modes; the only product from the Cu^{II}/NCO^-/HL ligand 'blend' is mononuclear.

The structural impact of the imidazole NH donor group on the supramolecular organization of the present crystal structures, in relation to the mononuclear complexes with the HL ligand reported in earlier studies,[35–38] deserves to be noted. In nearly all compounds, whether discrete or polymeric, the NH groups are involved in synthon formation, either through direct intermolecular interactions or mediated by counterions. In a few cases where such interactions are sterically hindered, suitably positioned and oriented crystallization solvents (*e.g.*, H_2O, Me_2CO, *etc.*) bridge the NH groups or form terminal H bonds with them. It is evident that the molecular self-assembly in all structures is effectively directed by recurring N–H···X synthons (X = halide, pseudohalide or solvent) irrespective of the structural type of the compound formed.

With the results and experience obtained in this work, our attempts are directed, among others, towards (1) efforts to prepare Cu^{II}/SCN^-/HL and $Cu^{II}/C(CN)_3^-$/HL complexes to investigate the influence of different pseudohalides on the product identity; (2) the use of other divalent 1st-row transition metals, *e.g.*, Mn^{II}, Fe^{II}, Co^{II} and Ni^{II}, in this chemistry with the aim to obtain coordination polymers with different structural types and magnetic properties; and (3) the replacement of HL with other heavily substituted imidazoles, *e.g.*, 1-methyl-4,5-diphenylimidazole (L), in order to explore their influence on the molecular structures of the Cu^{II}/X^-/imidazole complexes [$X^- = N_3^-$, $N(CN)_2^-$, NCO^-, *etc.*], but mainly to investigate the absence of hydrogen at N1 on the supramolecular motifs of the products that are expected to be different from those observed in the present study. Studies on perspectives 2 and 3, mentioned above, are advanced and will be submitted in due course. The ID polymeric complexes $\{[Co(N_3)_2(HL)]\}_n$ and $\{[Cu(N_3)_2(L)]\}_n$ have been structurally characterized (Fig. S7 and S8), and the study of their properties is in progress.

Author contributions

Evangelia-Spyridoula Fotopoulou: data curation, formal analysis, investigation, and methodology; Nikos Panagiotou: data curation, formal analysis, and investigation; Anastasios J. Tasiopoulos: formal analysis and methodology; Mark M. Turnbull: data curation, formal analysis, and software editing – original draft; Spyros P. Perlepes: conceptualization, investigation, methodology, writing – original draft, and supervision; Vassilios Nastopoulos: conceptualization, investigation, writing – original draft, supervision, review and editing.

Conflicts of interest

There are no conflicts to declare.

Data availability

The authors declare that the data supporting the findings of this study are available within the paper and its SI: structural schemes (Scheme S1), figures (Fig. S1–S4, S7 and S8) and tables (Tables S1–S4), and magnetic plots (Fig. S5 and S6). See DOI: **https://doi.org/10.1039/d5dt01389e**.

CCDC 2456934–2456936 contain the supplementary crystallographic data for this paper.[80a–c]

References

1 J. L. Burmeister, *Coord. Chem. Rev.*, 1990, **105**, 77–133.
2 A. Escuer, J. Esteban, S. P. Perlepes and T. C. Stamatatos, *Coord. Chem. Rev.*, 2014, **275**, 87–129.
3 S. R. Gottam, C.-T. Tsai, L.-W. Wang, C.-Y. Li, C.-C. Lin and S.-Y. Chu, *J. Electrochem. Soc.*, 2020, **167**, 027513.
4 M. K. Chattopadhyay, P. Ghorai, S. Datta, N. C. Jana and P. Banerjee, *Cryst. Growth Des.*, 2024, **24**, 5781–5793.
5 P. Ghorai, A. Dey, A. Hazra, B. Dutta, P. Brandão, P. P. Ray, P. Banerjee and A. Saha, *Cryst. Growth Des.*, 2019, **19**, 6431–6447.
6 A. R. Jeong, J. W. Shin, J. H. Jeong, S. Jeoung, H. R. Moon, S. Kang and K. S. Min, *Inorg. Chem.*, 2020, **59**, 15987–15999.
7 E. Coronado and P. Day, *Chem. Rev.*, 2004, **104**, 5419–5448.
8 D. R. Talham, *Chem. Rev.*, 2004, **104**, 5479–5501.
9 M. Boukabene, H. Brahim, D. Hadji and A. Guendouzi, *Theor. Chem. Acc.*, 2020, **139**, 47.
10 K. Kumar, O. Stefanczyk, K. Nakabayashi, K. Imoto, Y. Oki and S.-i. Ohkoshi, *Adv. Opt. Mater.*, 2022, **10**, 2101721.
11 J. Hossain, J. S. Gopinath, S. Tothadi, P. Parameswaran and S. Khan, *Organometallics*, 2022, **41**, 3706–3717.

12 E. B. Anderson and M. R. Buchmeiser, *Synlett*, 2012, **23**, 185–207.
13 A. K. Boudalis, Y. Sanakis, J. M. Clemente-Juan, B. Donnadieu, V. Nastopoulos, A. Mari, Y. Coppel, J.-P. Tuchagues and S. P. Perlepes, *Chem. – Eur. J.*, 2008, **14**, 2514–2526.
14 T. C. Stamatatos, K. A. Abboud, A. Wernsdorfer and G. Christou, *Inorg. Chem.*, 2009, **48**, 807–809.
15 D. I. Alexandropoulos, L. Cunha-Silva, A. Escuer and T. C. Stamatatos, *Chem. – Eur. J.*, 2014, **20**, 13860–13864.
16 O. Sato, J. Tao and Y.-Z. Zhang, *Angew. Chem., Int. Ed.*, 2007, **46**, 2152–2187.
17 P. Gütlich, Y. Garcia and T. Woike, *Coord. Chem. Rev.*, 2001, **219–221**, 839–879.
18 A. Escuer and G. Aromí, *Eur. J. Inorg. Chem.*, 2006, 4721–4736.
19 J. Ribas, A. Escuer, M. Monfort, R. Vicente, R. Cortes, L. Lezama and T. Rojo, *Coord. Chem. Rev.*, 1999, **193–195**, 1027–1068.
20 X.-Y. Wang, Z.-M. Wang and S. Gao, *Chem. Commun.*, 2008, 281–294.
21 T. C. Stamatatos and G. Christou, *Inorg. Chem.*, 2009, **48**, 3308–3322.
22 G.-C. Guo and T. C. W. Mak, *Angew. Chem., Int. Ed.*, 1998, **37**, 3268–3270.
23 S. R. Batten and K. S. Murray, *Coord. Chem. Rev.*, 2003, **246**, 103–130.
24 G. S. Papaefstathiou, A. Escuer, F. A. Mautner, C. Raptopoulou, A. Terzis, S. P. Perlepes and R. Vicente, *Eur. J. Inorg. Chem.*, 2005, 879–893.
25 J. Kohout, L. Jäger, M. Hvastijová and J. Kožišek, *J. Coord. Chem. Rev.*, 2000, **51**, 169–218.
26 F. A. Mautner, P. Jantscher, R. C. Fischer, A. Torvisco, R. Vicente, T. N. V. Karsili and S. S. Massoud, *Magnetochemistry*, 2019, **5**, 41.
27 N. de la Pinta, S. Martin, M. K. Urtiaga, M. G. Barandika, M. I. Arriortuo, L. Lezama, G. Madariaga and R. Cortés, *Inorg. Chem.*, 2010, **49**, 10445–10454.
28 A. Escuer, F. A. Mautner, N. Sanz and R. Vicente, *Inorg. Chem.*, 2000, **39**, 1668–1673.
29 A. H. Norbury, *Adv. Inorg. Chem. Radiochem.*, 1975, **17**, 231–386.
30 F. Meyer, E. Kaifer, P. Kircher, K. Heinze and H. Pritzkow, *Chem. – Eur. J.*, 1999, **5**, 1617–1630.
31 J. Martínez-Lillo, D. Armentano, G. De Munno, F. Lloret, M. Julve and J. Faus, *Inorg. Chim. Acta*, 2006, **359**, 4343–4349.
32 M. H. Sadhu and S. B. Kumar, *Polyhedron*, 2017, **123**, 419–429.
33 F. A. Mautner, M. Scherzer, C. Berger, R. C. Fischer, R. Vicente and S. S. Massoud, *Polyhedron*, 2015, **85**, 20–26.
34 Effendy, C. Di Nicola, M. Fianchini, C. Pettinari, B. W. Skelton, N. Somers and A. H. White, *Inorg. Chim. Acta*, 2005, **358**, 763–795.
35 K. A. Kounavi, C. Papatriantafyllopoulou, A. J. Tasiopoulos, S. P. Perlepes and V. Nastopoulos, *Polyhedron*, 2009, **28**, 3349–3355.
36 K. A. Kounavi, M. J. Manos, E. Moushi, C. Papatriantafyllopoulou, A. J. Tasiopoulos and V. Nastopoulos, *Cryst. Growth Des.*, 2012, **12**, 429–444.
37 K. A. Kounavi, E. Moushi, M. J. Manos, C. Papatriantafyllopoulou, A. J. Tasiopoulos and V. Nastopoulos, *CrystEngComm*, 2012, **14**, 6492–6502.
38 K. A. Kounavi, A. A. Kitos, E. Moushi, M. J. Manos, C. Papatriantafyllopoulou, A. J. Tasiopoulos, S. P. Perlepes and V. Nastopoulos, *CrystEngComm*, 2015, **17**, 7510–7521.
39 M.-I. Delegkou, N. Panagiotou, C. Papatriantafyllopoulou, A. J. Tasiopoulos, D. Papaioannou, S. P. Perlepes and V. Nastopoulos, *CrystEngComm*, 2024, **26**, 3574–3592.
40 E. Loukopoulos, E. Moushi, C. Papatriantafyllopoulou, A. A. Kitos, A. J. Tasiopoulos, S. P. Perlepes and V. Nastopoulos, *Acta Crystallogr., Sect. B: Struct. Sci., Cryst. Eng. Mater.*, 2024, **80**, 347–359.
41 E. C. Constable, *Metals and Ligand Reactivity: An Introduction to the Organic Chemistry of Metal Complexes*, VCH, Weinheim, Germany, 1996, pp. 240–245.
42 S.-S. Chen, *CrystEngComm*, 2016, **18**, 6543–6565.
43 S. J. Lippard and J. M. Berg, *Principles of Bioinorganic Chemistry*, University Science Books, Mill Valley, California, USA, 1994.
44 R. M. Roat-Malone, *Bioinorganic Chemistry*, Wiley, New Jersey, USA, 2002.
45 G. R. Desiraju, *Angew. Chem., Int. Ed. Engl.*, 1995, **34**, 2311–2327.
46 C. B. Aakeröy, N. R. Champness and C. Janiak, *CrystEngComm*, 2010, **12**, 22–43.
47 J. D. Dunitz and A. Gavezzotti, *Cryst. Growth Des.*, 2012, **12**, 5873–5877.
48 X.-J. Yang, F. Drepper, B. Wu, W.-H. Sun, W. Haehnel and C. Janiak, *Dalton Trans.*, 2005, 256–267.
49 J. G. Malecki, *J. Coord. Chem.*, 2011, **64**, 390–399.
50 X. Zhang, S. Li, Y.-J. He, T. Han, X.-L. Wang, B. Chen, K.-Y. Zou and Z.-X. Li, *Z. Anorg. Allg. Chem.*, 2015, **641**, 1874–1880.
51 D. Reinen, *Comments Inorg. Chem.*, 1983, **2**, 227–246.
52 F. A. Cotton, G. Wilkinson, C. A. Murillo and M. Bochmann, *Advanced Inorganic Chemistry*, Wiley, New York, USA, 6th edn, 1999, pp. 854–876.
53 *CrysAlis PRO, ver. 1.171.39.46*, Rigaku Oxford Diffraction, Yarnton, UK, 2018.
54 A. Altomare, G. Cascarano, C. Giacovazzo, A. Guagliardi, M. C. Burla, G. Polidori and M. Camalli, *J. Appl. Crystallogr.*, 1994, **27**, 435.
55 G. M. Sheldrick, *Acta Crystallogr., Sect. A: Found. Adv.*, 2015, **71**, 3–8.
56 L. Palatinus and G. Chapuis, *J. Appl. Crystallogr.*, 2007, **40**, 786–790.
57 L. Palatinus, S. J. Prathapa and S. van Smaalen, *J. Appl. Crystallogr.*, 2012, **45**, 575–580.
58 G. M. Sheldrick, *Acta Crystallogr., Sect. C: Struct. Chem.*, 2015, **71**, 3–8.
59 A. L. Spek, *Acta Crystallogr., Sect. D: Biol. Crystallogr.*, 2009, **65**, 148–155.

60 O. V. Dolomanov, L. J. Bourhis, R. J. Gildea, J. A. K. Howard and H. Puschmann, *J. Appl. Crystallogr.*, 2009, **42**, 339–341.
61 L. J. Farrugia, *J. Appl. Crystallogr.*, 2012, **45**, 849–854.
62 C. F. Macrae, I. Sovago, S. J. Cottrell, P. T. A. Galek, P. McCabe, E. Pidcock, M. Platings, G. P. Shields, J. S. Stevens, M. Towler and P. A. Wood, *J. Appl. Crystallogr.*, 2020, **53**, 226–235.
63 A. W. Addison, T. N. Rao, J. Reedijk, J. van Rijn and G. C. Verschoor, *J. Chem. Soc., Dalton Trans.*, 1984, 1349–1356.
64 L. Yang, D. R. Powell and R. P. Houser, *Dalton Trans.*, 2007, 955–964.
65 K. Nakamoto, *Infrared and Raman Spectra of Inorganic and Coordination Compounds*, 4th edn, Wiley, New York, USA, 1986, pp. 388–390.
66 A. Escuer, M. A. S. Goher, F. A. Mautner and R. Vicente, *Inorg. Chem.*, 2000, **39**, 2107–2112.
67 T. C. Stamatatos, G. S. Papaefstathiou, L. R. MacGillivray, A. Escuer, R. Vicente, E. Ruiz and S. P. Perlepes, *Inorg. Chem.*, 2007, **46**, 8843–8850.
68 L. K. Thomson and S. S. Tandon, *Comments Inorg. Chem.*, 1996, **18**, 125–144.
69 C. Adamo, V. Barone, A. Bencini, F. Totti and I. Ciofini, *Inorg. Chem.*, 1999, **38**, 1996–2004.
70 E. Ruiz, J. Cano, S. Alvarez and P. Alemany, *J. Am. Chem. Soc.*, 1998, **120**, 11122–11129.
71 K. Matsumoto, S.-I. Ooi, K. Nakatsuka, W. Mori, S. Suzuki, A. Nakahara and Y. Nakao, *J. Chem. Soc., Dalton Trans.*, 1985, 2095–2100.
72 L. Li, D. Liao, Z. Jiang and S. Yan, *Polyhedron*, 2001, **20**, 681–684.
73 J. P. Costes, F. Dahan, J. Ruiz and J. P. Laurent, *Inorg. Chim. Acta*, 1995, **239**, 53–59.
74 H. H. Hammud, U. Kortz, S. Bhattacharya, S. Demirdjian, E. Hariri, S. Isber, E. S. Choi, B. Mirtamizdoust, M. Mroueh and C. F. Daher, *Inorg. Chim. Acta*, 2020, **506**, 119533.
75 P. Manikandan, R. Muthukumaran, K. R. J. Thomas, B. Varghese, G. V. R. Chandramouli and P. T. Manoharan, *Inorg. Chem.*, 2001, **40**, 2378–2389.
76 J.-P. Zhao, Y. Xie, J.-R. Li and X.-H. Bu, *Dalton Trans.*, 2016, **45**, 1514–1524.
77 M. A. S. Goher, A. E. H. Abdou, M. A. M. Abu-Youssef and F. A. Mautner, *Transition Met. Chem.*, 2001, **26**, 39–43.
78 M. A. S. Goher, F. A. Mautner and N. A. Al-Salem, *Polyhedron*, 1997, **16**, 2239–2248.
79 M. A. S. Goher and F. A. Mautner, *Polyhedron*, 1998, **17**, 1561–1570.
80 (*a*) E.-S. Fotopoulou, N. Panagiotou, A. J. Tasiopoulos, M. M. Turnbull, S. P. Perlepes and V. Nastopoulos, CCDC 2456934: Experimental Crystal Structure Determination, 2025, DOI: **10.5517/ccdc.csd.cc2ngmyq**; (*b*) E.-S. Fotopoulou, N. Panagiotou, A. J. Tasiopoulos, M. M. Turnbull, S. P. Perlepes and V. Nastopoulos, CCDC 2456935: Experimental Crystal Structure Determination, 2025, DOI: **10.5517/ccdc.csd.cc2ngmzr**; (*c*) E.-S. Fotopoulou, N. Panagiotou, A. J. Tasiopoulos, M. M. Turnbull, S. P. Perlepes and V. Nastopoulos, CCDC 2456936: Experimental Crystal Structure Determination, 2025, DOI: **10.5517/ccdc.csd.cc2ngn0t**.